Rowe, R. K. & Li, A. L. (2002). *Géotechnique* **52**, No. 1, 29–40

Behaviour of reinforced embankments on soft rate-sensitive soils

R. K. ROWE* and A. L. LI*

The behaviour of reinforced embankments constructed over rate-sensitive soft foundation soils is studied. Factors such as the viscoplastic properties and hydraulic conductivity of the soil, reinforcement stiffness and construction rate are examined. The time-dependent responses of excess pore pressures, reinforcement strains and foundation deformations are investigated. The short-term embankment stability is of particular interest. The construction of reinforced embankments to the height determined based on a limit equilibrium design is simulated to examine the assumptions made in the conventional undrained analysis. It is shown that creep and stress-relaxation of viscoplastic soils after the end of embankment construction may be significant for rate-sensitive soils. The embankment stability is shown to be critical during creep and stress-relaxation of foundation soils after construction. The undrained shear strength measured in laboratory triaxial tests using currently recommended strain rates without an appropriate correction may lead to unsafe design for rate-sensitive soils. For such soils, the increase in reinforcement strain shortly after the completion of construction can be higher than that developed during the construction. Excess pore pressures increase after construction owing to the viscoplastic behaviour of the foundation soil. Reinforcement is shown to have the potential to both increase stability and decrease long-term creep deformations.

KEYWORDS: creep; embankments; geosynthetics; numerical modelling and analysis; reinforced soils; time dependence.

Nous étudions le comportement des berges renforcées construites sur des sols de fondation tendres et sensibles à la vitesse. Nous examinons des facteurs tels que les propriétés viscoplastiques et la conductivité hydraulique du sol, la rigidité du renforcement et la vitesse de construction. Nous recherchons les réponses en fonction du temps des pressions interstitielles excessives, des contraintes de renforcement et des déformations des fondations. La stabilité à court terme des berges présente un intérêt particulier. Nous simulons la construction de berges renforcées à la hauteur déterminée en nous basant sur une conception d'équilibre limite pour examiner les suppositions faites dans les analyses conventionnelles non drainées. Nous montrons que le fluage et la relaxation-tension des sols viscoplastiques à la fin de la construction des berges peuvent avoir une signification particulière pour les sols sensibles à la vitesse. Nous montrons que la stabilité des berges est critique pendant le fluage et la relaxation-tension des sols de fondation après la construction. La résistance au cisaillement non drainé, mesurée lors d'essais triaxiaux en laboratoire et utilisant les taux de contraintes recommandés actuellement sans une correction appropriée, peut conduire à une conception non fiable dans le cas de sols sensibles à la vitesse. Pour ces sols, l'augmentation de la contrainte de renforcement peu de temps après l'achèvement de la construction, peut être plus élevée que celle développée pendant la construction. Les pressions interstitielles excessives augmentent après la construction en raison du comportement viscoplastique du sol de fondation. Nous montrons que le renforcement a le potentiel à la fois d'augmenter la stabilité et de réduire les déformations du fluage à long terme.

INTRODUCTION

Although considerable attention has been paid to the behaviour and design of reinforced embankments on rate-insensitive soils (e.g. Ingold, 1982; Rowe & Soderman, 1985, 1987; Fowler & Koerner, 1987; Leshchinsky, 1987; Jewell, 1996; Sharma & Bolton, 1996; Holtz *et al.*, 1997; Rowe & Li, 1999), the time-dependent behaviour of geosynthetic reinforced embankments over rate-sensitive soft clay foundations has received little attention in the literature. This paper attempts to provide some insight into the potential effects of the viscous nature of soft cohesive foundation soils on the short-term stability of reinforced embankments. It is well known that natural soft cohesive soil deposits exhibit significant time-dependent behaviour, and the undrained shear strength of natural soft clays is strain-rate-dependent (e.g. Casagrande & Wilson, 1951; Bjerrum, 1972; Lo & Morin, 1972; Graham *et al.*, 1983; Leroueil & Marques, 1996; Sheahan *et al.*, 1996).

Under embankment loading, the excess pore pressure and deformation response of rate-sensitive foundation soft soils are often reported to be anomalous compared with the response described or predicted by the classical consolidation theory. For example, during the second-stage construction of the Gloucester test fill, the excess pore pressure increased owing to the creep of the foundation soil (Fisher *et al.*, 1982). Rowe *et al.* (1996) showed that at the Sackville test site substantial vertical and horizontal displacements were recorded in the absence of pore pressure dissipation during periods of a constant embankment load. Kabbaj *et al.* (1988) and Crooks *et al.* (1984) reported that, in a number of field cases they examined, the excess pore pressure in the foundation soils continued to increase significantly following completion of loading, or insignificant pore-water pressure dissipation occurred for long periods following construction. To predict embankment performance on many soft cohesive soils it is important to model the viscous behaviour of the soil (Gibson & Lo, 1961; Lo *et al.*, 1976; Fisher *et al.*, 1982; Leroueil & Marques, 1996; Rowe & Hinchberger, 1998). However, only a few investigators (e.g. Helwany & Wu, 1995; Rowe & Hinchberger, 1998) have investigated the behaviour of reinforced soil structures constructed over viscous foundation soils. The influence of the viscoplastic nature of soft clays on the interaction of soil and reinforcement is not well understood, and no consideration is given to the time-dependent behaviour of cohesive soils in current design methods for reinforced embankments.

This paper examines the construction of reinforced embankments over rate-sensitive soft foundation soils, using the finite element technique. The short-term stability of reinforced embankments and soil–reinforcement interaction are the items of major interest. The influence of factors such as the viscoplastic properties and hydraulic conductivity of soils, reinforcement stiffness and construction rate will be examined. Particular attention is given to the development of reinforcement strain and excess pore pressures in the foundation soils.

Manuscript received 2 February 2001; revised manuscript accepted 30 October 2001.
Discussion on this paper closes 1 August 2002, for further details see p. ii.
*Department of Civil Engineering, Queen's University, Kingston, Ontario, Canada

FINITE ELEMENT MODELLING OF REINFORCED EMBANKMENTS

The finite element program AFENA (Carter & Balaam, 1990), modified to allow modelling of soil–reinforcement interaction along the lines described by Rowe & Soderman (1985), is adopted in this paper to simulate the embankment construction. The results to be presented were obtained for embankments with a 15–21 m wide crest and 2h:1v side slopes overlying a 15 m soft cohesive deposit overlying a relatively rigid and permeable sand layer (see Fig. 1). Fig. 1 also shows the finite element mesh including a total of 1594 six-noded linear strain triangular elements (3516 nodes) used to discretise the embankment and foundation soils. The centreline of the embankment and the far field lateral boundary were taken to be smooth and rigid, with the lateral boundary located 100 m from the centreline. The bottom of the finite element mesh was assumed to be rough and rigid, and zero excess pore pressures were assigned to the nodes along the bottom boundary line. Embankment construction was simulated by gradually turning on the gravity of the embankment in 0·75 m thick lifts at a rate corresponding to the embankment construction rate.

Constitutive model for rate-sensitive cohesive soils and soil properties examined

The adopted elasto-viscoplastic soil model fully coupled with Biot consolidation theory (Biot, 1941) can describe not only inviscid behaviour, such as consolidation and strain hardening, but also viscous behaviour, such as rate sensitivity, creep and stress relaxation of the soft foundation soils under embankment loadings. The model and computer program used to obtain the results presented in this paper have previously been successfully used to predict both short-term and long-term field behaviour, including the behaviour of a geotextile-reinforced embankment constructed over the rate-sensitive Sackville foundation soil (Rowe & Hinchberger, 1998) and the behaviour of an unreinforced embankment constructed over the rate-sensitive Gloucester foundation soil (Hinchberger & Rowe, 1998). The constitutive theory is based on overstress viscoplasticity (Perzyna, 1963) and an elliptical yield cap model proposed by Chen & Mizuno (1990). The main features of the model are summarised in the following text and in Fig. 2. Additional details regarding the model are provided by Hinchberger (1996) and Rowe & Hinchberger (1998).

The yield surface of the elliptical cap model shown in Fig. 2 in $\sigma'_m - \sqrt{2J_2}$ stress space (where σ'_m is the mean effective stress and J_2 is the second invariant of the deviatoric stress tensor) can be characterised in terms of: R, which is the yield surface aspect ratio in σ'_m–$\sqrt{2J_2}$ stress space; l, which is the mean effective stress corresponding to the centre of the ellipse; and $\sigma'^{(s)}_y$, $\sigma'^{(d)}_y$, which are the intercepts with the σ'_m axis (i.e. the size) of the static and dynamic (associated with a stress state) yield envelopes respectively. The failure is governed by the Drucker–Prager failure criterion, having a slope $M_{N/C}$ and $M_{O/C}$ for the normally and overconsolidated failure envelopes respectively.

Since the deposition of the foundation soil it has experienced 'ageing' due to the secondary compression, which has resulted in a higher preconsolidation pressure than the initial vertical effective stress (Bjerrum, 1972). This preconsolidation pressure is considered as the static preconsolidation pressure in the viscoplastic model. The stress state point, A_i shown in Fig. 2, represents an initially slightly overconsolidated point within a clayey foundation having a mean static preconsolidation pressure $\sigma'^{(s)}_{yA}$ and an earth pressure coefficient at rest K'_0. With rapid embankment loading, the stress path moves vertically in an elastic undrained manner towards point A on the yield surface. After the soil yields, it moves along a series of dynamic yield envelopes and reaches point B, where the soil is overstressed by an amount $\sigma'^{(d)}_{os}$, and the positive viscoplastic volumetric strains expand the static yield envelope from $\sigma'^{(s)}_{yA}$ to $\sigma'^{(s)}_{yB}$ at the end of construction. After the end of construction and before significant consolidation, creep and stress-relaxation of the soil skeleton cause the stress path to move from point B to C, and the static yield envelope expands from $\sigma'^{(s)}_{yB}$ to $\sigma'^{(s)}_{yC}$ owing to the positive viscoplastic volumetric strains. The consequent plastic deformation and excess pore pressure are functions of the overstress and the location of the stress state point on the dynamic yield envelope. The stress path A–C represents the possible stress path when the soil is under a slow embankment loading.

The total strain-rate tensor, $\dot{\varepsilon}_{ij}$ of the elasto-viscoplastic soil is expressed as

$$\dot{\varepsilon}_{ij} = \dot{\varepsilon}^{e}_{ij} + \dot{\varepsilon}^{vp}_{ij} \tag{1}$$

where $\dot{\varepsilon}^{e}_{ij}$ is the elastic strain-rate tensor and $\dot{\varepsilon}^{vp}_{ij}$ is the viscoplastic strain-rate tensor.

The elastic strain tensor, $\dot{\varepsilon}^{e}_{ij}$, is governed by the elastic bulk modulus K and shear modulus G, which are given by

$$K = \frac{1+e}{\kappa}\sigma'_m \tag{2}$$

$$G = \frac{3(1-2\nu')K}{2(1+\nu')} \tag{3}$$

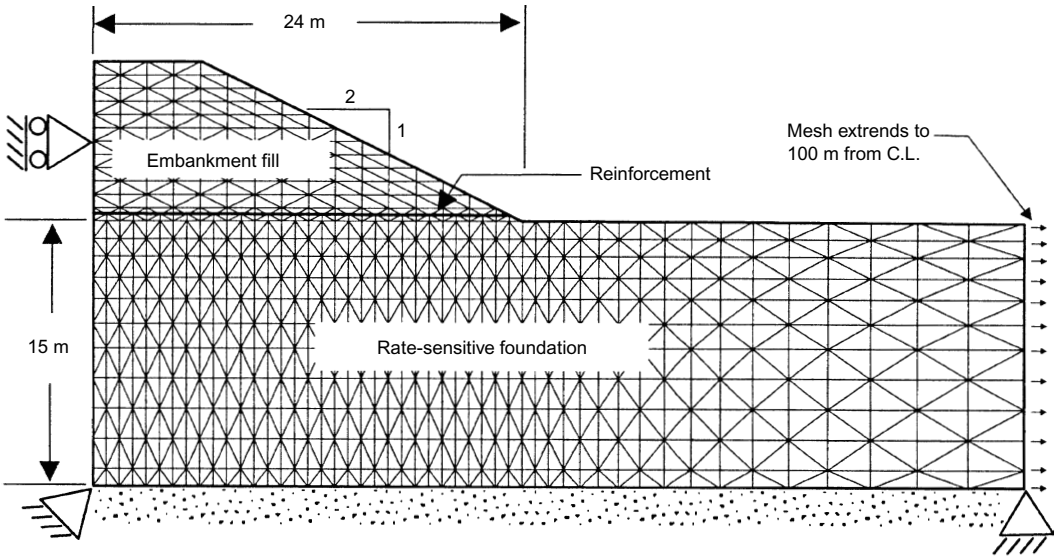

Fig. 1. The finite element mesh and geometry of the system

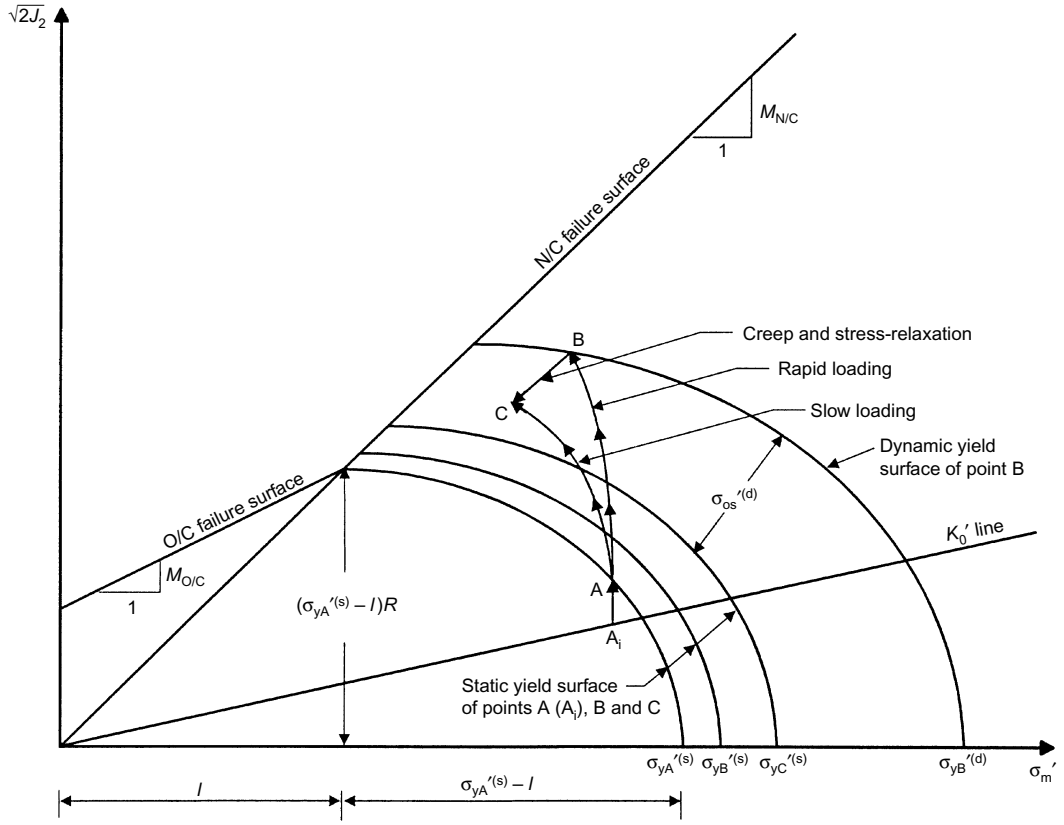

Fig. 2. Elasto-viscoplastic elliptical cap soil model (modified from Rowe & Hinchberger 1998)

where σ'_m is the mean effective stress, e is the void ratio, κ is the recompression index in the e–$\ln(\sigma'_m)$ space, and ν' is Poisson's ratio. The viscoplastic strain-rate tensor, $\dot{\varepsilon}_{ij}^{vp}$, is given by

$$\dot{\varepsilon}_{ij}^{vp} = \gamma^{vp}\langle\Phi(F)\rangle\frac{\partial f}{\partial\sigma'_{ij}} \tag{4}$$

where γ^{vp} is the viscoplastic fluidity parameter with units of inverse time, f is the plastic potential function that equals the elliptical cap yield function or the Drucker–Prager failure function using an associated flow rule, and $\Phi(F)$ is the flow function, defined as follows:

$$\Phi(F) = \left(\frac{\sigma_y'^{(s)} + \sigma_{os}'^{(d)}}{\sigma_y'^{(s)}}\right)^n \tag{5}$$

where n is the strain-rate exponent.

Two rate-sensitive soft foundations, denoted as soils C-R1 and C-R2, were examined. The elasto-viscoplastic model parameters are summarised in Table 1. Soil C-R1 had properties similar to the Sackville soil described by Rowe & Hinchberger (1998), and the soil parameters given in Table 1 were based on the values in the upper 14 m of the Sackville deposit. The average liquid limit, plasticity index and natural water content were approximately 50%, 18% and 53% respectively. The viscosity constants, γ^{vp} and n, and the strength parameters of Sackville soil were estimated from a combination of constant-rate CAU triaxial tests and CAU triaxial creep tests (see Hinchberger, 1996 for the details of the test results). Fig. 3 shows the profile of the static preconsolidation pressure, σ'_p, that was adopted. Since the upper layers of natural clayey deposits often have a preconsolidation pressure significantly higher than the initial vertical effective stress, owing to the effects of weathering and ground water fluctuation, the deposit was assumed to be slightly overconsolidated, having a 2 m thick crust (see Fig. 3) and, below the first 2 m, an OCR of 2·4–1·1 calculated on the basis of the static preconsolidation pressure and initial effective vertical stress. The values of K'_0 typically vary with OCR (Kulhawy & Mayne, 1990). However, preliminary calculations showed that typical changes in K'_0 with OCR did not have a significant effect on the deformations and stability of the embankment, and hence for simplicity in the analyses reported herein K'_0 was assumed to be constant (at 0·75) with depth. Based on the viscoplastic model and adopting the parameters given in Table 1, finite element simulations of CAU triaxial tests were performed at different strain rates. Fig. 4 shows that for soil C-R1 the calculated undrained shear strength increases by about 16% per logarithm cycle of strain rate for strain rates between 0·005%/h and 100%/h, and there is essentially no change in strength with strain rate for rates less than 0·005%/h. The viscous behaviour of soil C-R1 is essentially the same as that of the Sackville rate-sensitive soil.

Table 1. Elliptical cap soil model parameters

Soil parameter	Soil C-R1	Soil C-R2
Failure envelope, $M_{N/C}(\phi')$	0·96 (29°)	0·96 (29°)
Failure envelope, $M_{O/C}$	0·75	0·75
Aspect ratio, R	1·25	1·25
Compression index, λ	0·16	0·16
Recompression index, κ	0·034	0·03
		4
Coefficient of earth pressure at rest, K'_0	0·75	0·75
Poisson's ratio, ν'	0·3	0·3
Unit weight, γ: kN/m^3	17	17
Initial void ratio, e_o	1·38–1·5	1·38–1·5
Viscoplastic fluidity, γ^{vp}: h^{-1}	$2{\cdot}0 \times 10^{-5}$	$1{\cdot}0^{-7}$
Strain-rate exponent, n	20	30

Kulhawy & Mayne (1990) compiled data obtained from 26 different overconsolidated and normally consolidated clays, and found that the average increase in undrained shear strength typically equalled 10% per logarithm cycle of strain rate, as shown in Fig. 4. Soil C-R2 was assumed to have the same

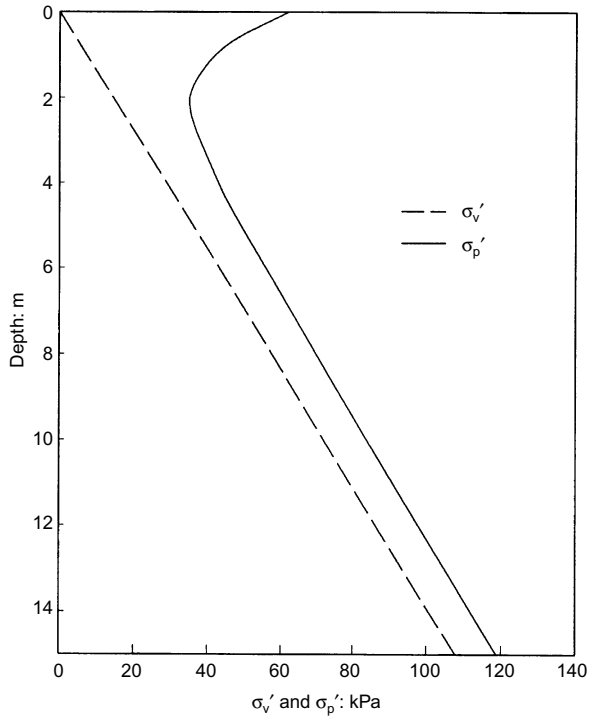

Fig. 3. Initial vertical effective stress and preconsolidation pressure profiles for both soils C-R1 and C-R2

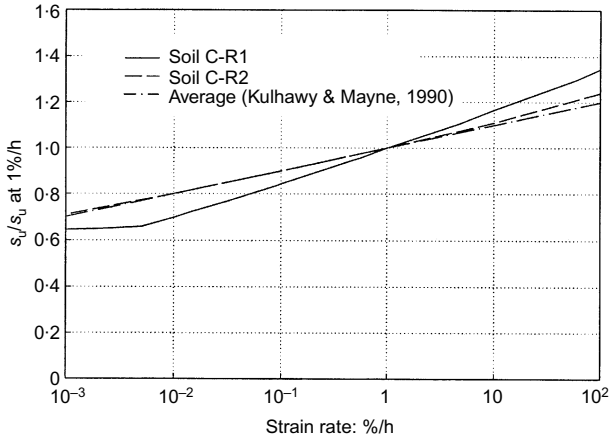

Fig. 4. The effect of strain rate on the undrained shear strength, s_u, of soils C-R1 and C-R2

properties as soil C-R1 except for the viscosity constants γ^{vp} and n. These two constants of soil C-R2 were back-calculated to capture the average strain-rate sensitivity of typical clayey soils reported by Kulhawy & Mayne (1990), and are given in Table 1. For a strain rate within the range of interest, the undrained shear strength of soil C-R2 is higher than that of soil C-R1 and is rate-sensitive for a strain rate as low as 0·001%/h, as shown in Fig. 4.

The hydraulic conductivity of soft clays was taken to be a function of void ratio:

$$k_v = k_{vo} \exp\left(\frac{e - e_o}{C_k}\right) \tag{6}$$

where k_{vo} is the reference hydraulic conductivity, and is either 2×10^{-9} m/s or 4×10^{-10} m/s; C_k is the hydraulic conductivity change index ($C_k = 0{\cdot}2$ here); and e_o is the reference void ratio (taken to be 1·5). The hydraulic conductivity was considered to be anisotropic with $k_h/k_v = 4$.

Embankment fill parameters and construction rates

An elastic perfectly plastic model with Mohr–Coulomb failure surface and the non-associated flow rule proposed by Davis (1968) was adopted for the granular embankment fill, which was assumed to be a purely frictional granular soil with friction angle, $\phi' = 37°$, dilatancy angle, $\psi = 6°$, and a unit weight, $\gamma = 20$ kN/m^3. The non-linear elastic behaviour of the fill was modelled using Janbu's (1963)

$$(E/P_a) = K_s(\sigma_3/P_a)^m \tag{7}$$

where E is the Young's modulus of the soil, P_a is the atmospheric pressure, σ_3 is the minor principal stress, and K and m are material constants taken to be 300 and 0·5 respectively. Two embankment construction rates, 2 m/month and 10 m/month, were examined.

Interface parameters and reinforcement stiffness

The geosynthetic reinforcement examined in the present paper was assumed not to have any significant flexural rigidity or time-dependent response, and was modelled using elastic bar elements with axial stiffness varying between 0 and 2000 kN/m. The effect of the time-dependent behaviour of non-linear-viscoelastic geosynthetic reinforcement (such as high-density polyethylene geogrids) will be addressed in a subsequent paper. The interaction between the soil mass and the reinforcement was modelled by soil–reinforcement interface elements with strength governed by the Mohr–Coulomb failure criterion (see Rowe & Soderman, 1987 for details). The fill–reinforcement interface was assumed to be frictional, with $\phi' = 37°$.

RESULTS AND DISCUSSIONS

Rate effect on embankment stability during construction

To investigate the effect of the rate-sensitive behaviour of soft soil on embankment stability during construction, an analysis was conducted to simulate the construction of unreinforced embankments over both elasto-viscoplastic foundation soil C-R1 and inviscous elastoplastic foundation soil C at a construction rate, CR, of 10 m/month. The inviscous soil had the same elliptical cap soil properties and hydraulic properties as those of the viscous soil. Therefore the undrained shear strength of the inviscous soil C is equal to what would be the undrained shear strength of viscous soil C-R1 if it were sheared at an extremely slow rate. Fig. 5 shows the calculated variation of net embankment height above the original ground surface with embankment fill thickness, where the embankment stability can be evaluated in terms of the failure height (i.e. the fill thickness corresponding to the peak net embankment height). Both embankments exhibited initial behaviour having an essentially linear initial response followed by a non-linear response and eventual failure

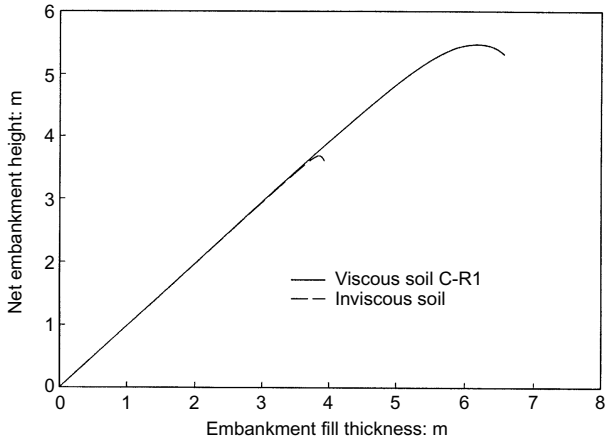

Fig. 5. The variation of net embankment height with fill thickness for the unreinforced embankment with $CR = 10$ m/month

at a fill thickness of 3·86 and 6·15 m for the inviscous and viscous foundation soils respectively. The failure of the embankment over the viscous soil was more ductile than that of the embankment over inviscous soil.

The results suggest that although both foundation soils had the same elastoplastic properties, the elasto-viscoplastic soil behaved like a much stronger soil owing to strain-rate effect in the foundation soil during embankment construction. For this particular rate-sensitive soil and construction rate, rate effects resulted in a 59% increase in the short-term failure height of an unreinforced embankment continuously constructed to failure relative to that for an otherwise similar but rate-insensitive soil. Hence it is evident that the undrained shear strength mobilised during the embankment construction is dependent on the viscous properties of the soil.

Rate effect on embankment stability after construction

An analysis was conducted to simulate the construction of an embankment to a height (fill thickness) selected on the basis of conventional soil parameters and a limit equilibrium analysis. The undrained shear strength obtained from different tests and strain rates will be different. To illustrate the effect, the undrained shear strengths deduced using K_0 consolidated undrained plane strain compression (CK_0 UPC) and triaxial compression (CK_0 UC) tests were used to assess stability. The effect of strain rate was also examined. The strain rates recommended in literature for undrained laboratory tests range from 2·4–4·8%/h (Bishop & Henkel, 1962) to 0·5–1%/h (Germaine & Ladd, 1988). For the purpose of this example both an upper strain rate of 4·8%/h (Bishop & Henkel, 1962) and a lower strain rate of 0·5%/h (Germaine & Ladd, 1988) were used to calculate the undrained shear strength profile of soil C-R1 for both plane strain and triaxial compression conditions.

For a 6·75 m thick embankment with reinforcement (see Fig. 1 for the location) having a tensile strength of 100 kN/m, the calculated ratio of the restoring moment to the overturning moment (i.e. the equilibrium ratio, ERAT) from a limit equilibrium program (Mylleville & Rowe, 1988) was 1·16 and 1·01 using the undrained shear strength profile based on CK_0 UPC tests at the 4·8%/h and 0·5%/h strain rates respectively, and 1·02 and 0·9 based on CK_0UC tests at 4·8%/h and 0·5%/h respectively. The limit equilibrium analysis based on plane strain shear strength implied that a 6·75 m high embankment should be marginally stable if reinforcement with a tensile stiffness, J, of 2000 kN/m and an allowable strain, ε_{all}, of 5% (to achieve the tensile force of 100 kN/m) were adopted.

For a 5·25 m thick embankment reinforced with reinforcing tensile force of 100 kN/m, the calculated equilibrium ratio was 1·41 and 1·24 using the undrained shear strength profile based on CK_0 UPC tests at 4·8%/h and 0·5%/h strain rate respectively and 1·25 and 1·09 based on CK_0 UC tests at 4·8%/h and 0·5%/h respectively. Thus the limit equilibrium analysis based on either the triaxial or plane strain shear strength implied that the 5·25 m high reinforced embankment should be stable.

Fig. 6 shows the development of maximum reinforcement strains for both the 6·75 m and 5·25 m reinforced embankments with $J = 2000$ kN/m. The location of the maximum reinforcement strain varied, moving from a location just behind the embankment shoulder at the end of construction (EOC) towards the centre of the embankment during consolidation. The results presented in Fig. 6 give strains during and shortly after the embankment construction for a construction rate, CR, of 10 m/month, assuming that the reinforcement could sustain the strain developed without breakage. In the case of the 6·75 m high embankment, the maximum reinforcement strain of 5·8% at the end of construction (EOC) exceeded the design limit of 5% based on the limit equilibrium analysis. Furthermore, it kept increasing after the end of construction and reached as high as 16% at time $t = 2500$ h (2·8 months after the end of construction at t = 486 hours). A strain of 16% would exceed the ultimate tensile strain for most high-strength geosynthetic products (Industrial Fabrics Association International, 1999). Thus the finite element analysis indicated that the reinforcement would fail some time after the construction of the 6·75 m high embankment, and that the embankment would collapse upon the failure of the reinforcement.

Also shown in Fig. 6 is the reinforcement strain mobilised during and after the construction of the 5·25 m high embankment. The maximum reinforcement strain developed at the end of construction was 1·7%, implying that the embankment would be stable at the end of construction. However, the reinforcement strain increased to 6% by $t = 2500$ hours (2·9 months after the construction at t = 378 hours). According to the limit equilibrium analysis based on either the CK_0UPC or the CK_0UC test at the lower strain rate (0·5%), the reinforcement strain should be less than 5% since the ratio of restoring to overturning moment (ERAT) was greater than 1·0 for the embankment with

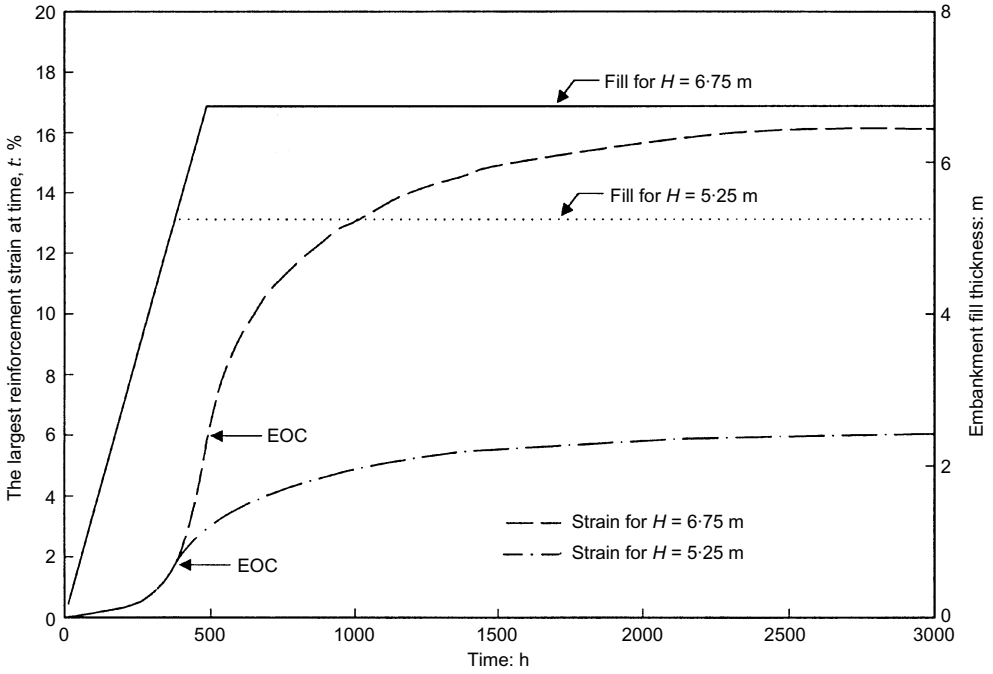

Fig. 6. Reinforcement strain developed during the short term for embankments with $CR = 10$ m/month, $J = 2000$ kN/m over soil C-R1

a reinforcing tensile force of 100 kN/m. Exceeding the allowable strain in the finite element analysis implies that the calculated stability in the limit equilibrium analysis is overestimated. It was found that the reinforced embankment (with $J = 2000$ kN/m) could be constructed to only 5 m height for a design reinforcement strain of 5%.

The results shown in Fig. 6 suggest that the undrained shear strength profile of the foundation soil that would be deduced at a strain rate of 4·8%/h or 0·5%/h for both plane strain and axisymmetric (triaxial) conditions would exceed that which could be mobilised in the field for the rate-sensitive soil examined. Therefore special care must be taken to choose the strain rate for use in the determination of undrained shear strength for these soils or to adjust the strength based on consideration of strain-rate effects. The conventional undrained analysis method usually makes an assumption that the embankment stability is critical at the end of construction. This assumption can lead to significant errors for rate-sensitive soils, as shown in Fig. 6. The stability may decrease with time after the end of construction owing to the viscous behaviour, as has been observed in several field cases (e.g. Crooks *et al.*, 1984; Keenan *et al.*, 1986).

Effects on reinforcement strains

Fig. 7 shows the variation in the maximum reinforcement strain with time during and after the construction of the 5 m high embankment over foundation soil C-R1. To also investigate partial drainage effects, three different conditions are considered. In Case I the construction rate (CR) was 10 m/month and the reference hydraulic conductivity, k_{v0}, was 2×10^{-9} m/s; in Case II $CR = 10$ m/month and $k_{v0} = 4 \times 10^{-10}$ m/s; and in Case III $CR = 2$ m/month and $k_{v0} = 2 \times 10^{-9}$ m/s. For Case I the maximum reinforcement strain at the end of construction was only 1·4%; it increased to 5% at $t = 4000$ h (5·6 months) after the end of construction at t = 360 hours owing to creep of the foundation soil. The significant increase of reinforcement strain after the end of construction due to the creep effects of rate-sensitive foundation soils was also observed in a field case reported by Rowe & Gnanendran (1994). It is evident in Fig. 7 that the maximum reinforcement strains developed both during and after construction were influenced by the rate of partial consolidation. For Case II, with the hydraulic conductivity of the foundation soil five times lower than in Case I, the maximum reinforcement strain was 5·5% at $t = 4000$ h, which was higher than for Case I even though the strain at the end of construction was the same (1·4%).

Fig. 7 shows the effect of a fivefold decrease in construction rate between Cases I and III. The reduction in construction rate resulted in a higher end-of-construction strain (e.g. 2·1% for Case III compared with 1·4% for Case I) but smaller long-term strain (e.g. 4·1% for Case III compared 5% for Case II at $t = 4000$ h). The increase in reinforcement strain at the end of construction can be attributed to the longer time period over which the foundation soil could creep during construction, and to the lower strain rate in the foundation soil resulting from the slower construction rate. However, the partial pore pressure dissipation during construction in Case III resulted in less time-dependent reinforcement strain after the end of construction than in Case I. For the cases examined here, the increase in reinforcement strain between the end of construction and 4000 h was 2·0%, 3·6% and 4%, which was 95%, 257% and 286% of the maximum strain at the end of construction for Cases III, I and II respectively.

To investigate the time-dependent reinforcement strain that arises from the different levels of rate-dependent behaviour of the foundation soil, an analysis was conducted for a 6 m high reinforced embankment with $J = 2000$ kN/m constructed over the foundation soil C-R2. Soil C-R2 is more rate-sensitive at slow strain rates and less sensitive at high strain rates than soil C-R1. It was found that a 6 m reinforced embankment could be stable over this foundation soil for the reinforcement considered and a construction rate of 10 m/month.

Fig. 8 shows the maximum reinforcement strain developed for the three different conditions examined for soil C-R2. The trends in Fig. 8 are similar to those in Fig. 7. There are, however, two major differences between Figs 7 and 8. The first is that the rate of increase in reinforcement strain was slower for embankments over soil C-R2 than for embankments over soil C-R1. The second is that the increase in reinforcement strain took longer to stabilise after construction for embankments over soil C-R2 than for embankments over soil C-R1. This is because, at the same construction rate, higher overstresses ($\sigma'^{(d)}_{os}$) were developed in soil C-R2 during construction than in soil C-R1 owing to the combined effects of the lower value of the viscosity parameter (γ^{vp}) for soil C-R2 and the higher embankment over soil C-R2. Consequently, creep and stress-relaxation of foundation soil C-R2 and the consequent

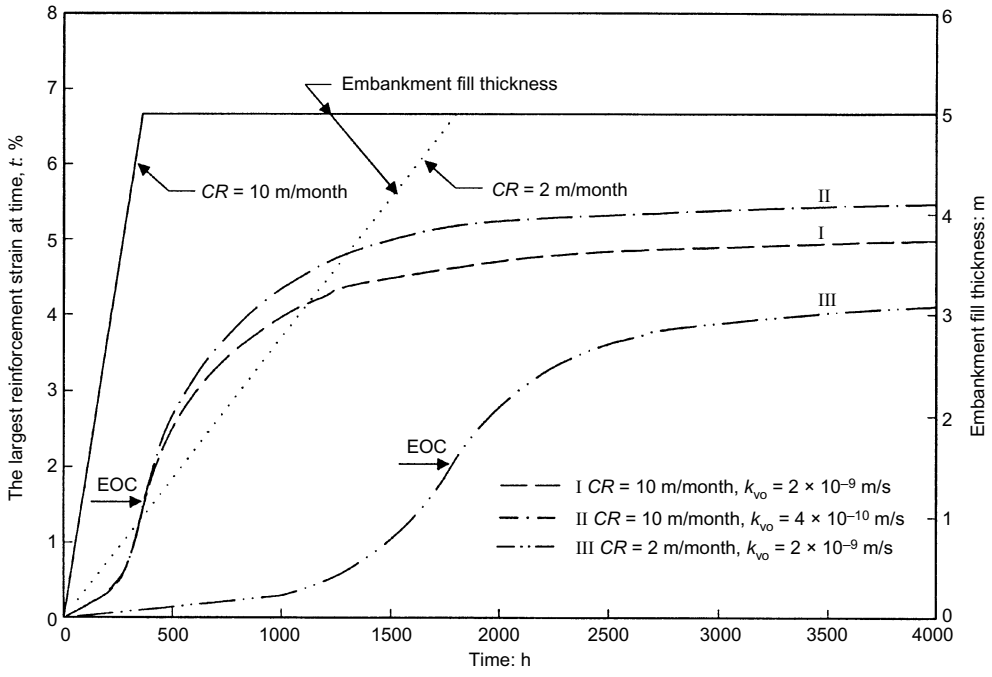

Fig. 7. Reinforcement strains developed for embankments over soil C-R1 ($H = 5$ m, $J = 2000$ kN/m)

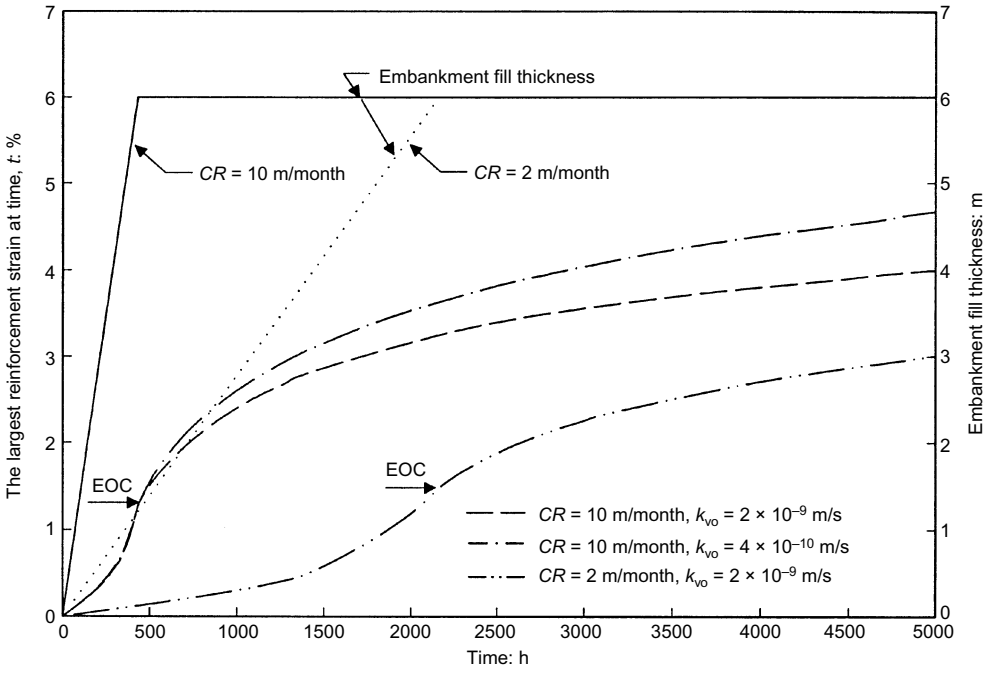

Fig. 8. Reinforcement strains developed for embankments over soil C-R2 ($H = 6$ m, $J = 2000$ kN/m)

viscoplastic shear deformations occurred over a longer period of time when overstresses gradually diminished and effective stresses reached equilibrium.

Li & Rowe (1999) have shown that when embankments are constructed over an inviscous foundation soil the reinforcement strains are mostly mobilised at the end of construction. However, for embankments constructed over a viscoplastic foundation soil the mobilised reinforcement strains at the end of construction (see Figs 6, 7 and Fig. 8) were relatively small, and most of the reinforcement strains were mobilised well after completion of embankment construction. The subsequent time-dependent reinforcement strain was a function of the viscoplastic properties of soils, the loading intensity, and the partial drainage conditions.

Effects on embankment deformations

Fig. 9 shows the calculated deformations at the embankment toe for the three embankments over soil C-R1 described in the previous section. The trend of the toe deformations is similar to that of the reinforcement strain (see Fig. 7). The construction deformations were small, while the time-dependent deformations were significant after construction owing to creep of the soil. The partial drainage associated with slower construction (Case III) significantly reduced the creep deformations owing to the dissipation of excess pore pressure and the consequent strength gain of the foundation soil during construction. From the calculation of the horizontal deformations of the foundation soil below the embankment toe at different times for Case I, the maximum horizontal displacement at the end of construction was computed to be 0·22 m, which was less than 19% of the calculated long-term maximum horizontal displacement at 15 years. The major creep displacements were found to develop during the first 4 months of the post-construction period.

Effects on excess pore pressures

Fig. 10 shows the maximum excess pore pressure developed at point X, 4·4 m below the embankment centreline, during and after the construction of the 6·75 m thick embankment (with 135 kPa vertical pressure) examined above in the section 'Rate effect on embankment stability after construction'. When the foundation soil had a hydraulic conductivity constant $k_{vo} = 2 \times 10^{-9}$ m/s, the excess pore pressure developed at point X was 130 kPa at the end of construction. Owing to the viscous response, it increased by another 12 kPa up to a total of 142 kPa at about 26 days (1100 hours) after the end of construction, which exceeded the embankment load by 7 kPa. Subsequently, the excess pore pressure slowly decreased owing to consolidation. Fig. 10 also shows that, when the foundation soil had a lower hydraulic conductivity ($k_{vo} = 4 \times 10^{-10}$ m/s), the excess pore pressure increased from 130 kPa at the end of construction to 147 kPa at about 34 days after the end of construction. The maximum pore pressure exceeded the embankment load by 12 kPa, and the excess pore pressure still remained above 140 kPa when the analysis was terminated some 3500 hours (more than 140 days) after it reached 140 kPa.

Fig. 11(a) shows the contours of the excess pore pressure for the 5 m thick reinforced embankment (Case I) on soil C-R1 19 days after construction, when the maximum excess pore pressure was developed in the foundation soil. Two observations can be made. The first is that the shape of the isochrone-like curves was modified by the shearing of soil below the embankment slope. The second is that the maximum pore pressure was developed at a location some distance away from the embankment centreline and not immediately below the centre as is usually expected. This is because the time-dependent development of excess pore pressure due to creep is a function not only of total external load but also of the shear intensity in the foundation soil.

The second point noted above is illustrated in Fig. 11(b), which shows the contours of the change in excess pore pressures between the end of construction and 19 days after the end of construction. In spite of some decrease at the top and bottom due to drainage boundary effects, the shape of the contours clearly suggests that the distribution of creep-induced excess pore pressure is affected by the shear direction of the foundation soil. The soil below the embankment slope, where the shearing was most intensive, had a greater increase in excess pore pressure during the post-construction period.

The location of maximum excess pore pressure developed in the foundation soil is also a function of the geometry of the embankment since it affects the total increase of applied pressure and the zone of most intensive shearing in the foundation soil. For example, in the case of the 6 m embankment over soil C-R2, the maximum post-construction pore pressure was

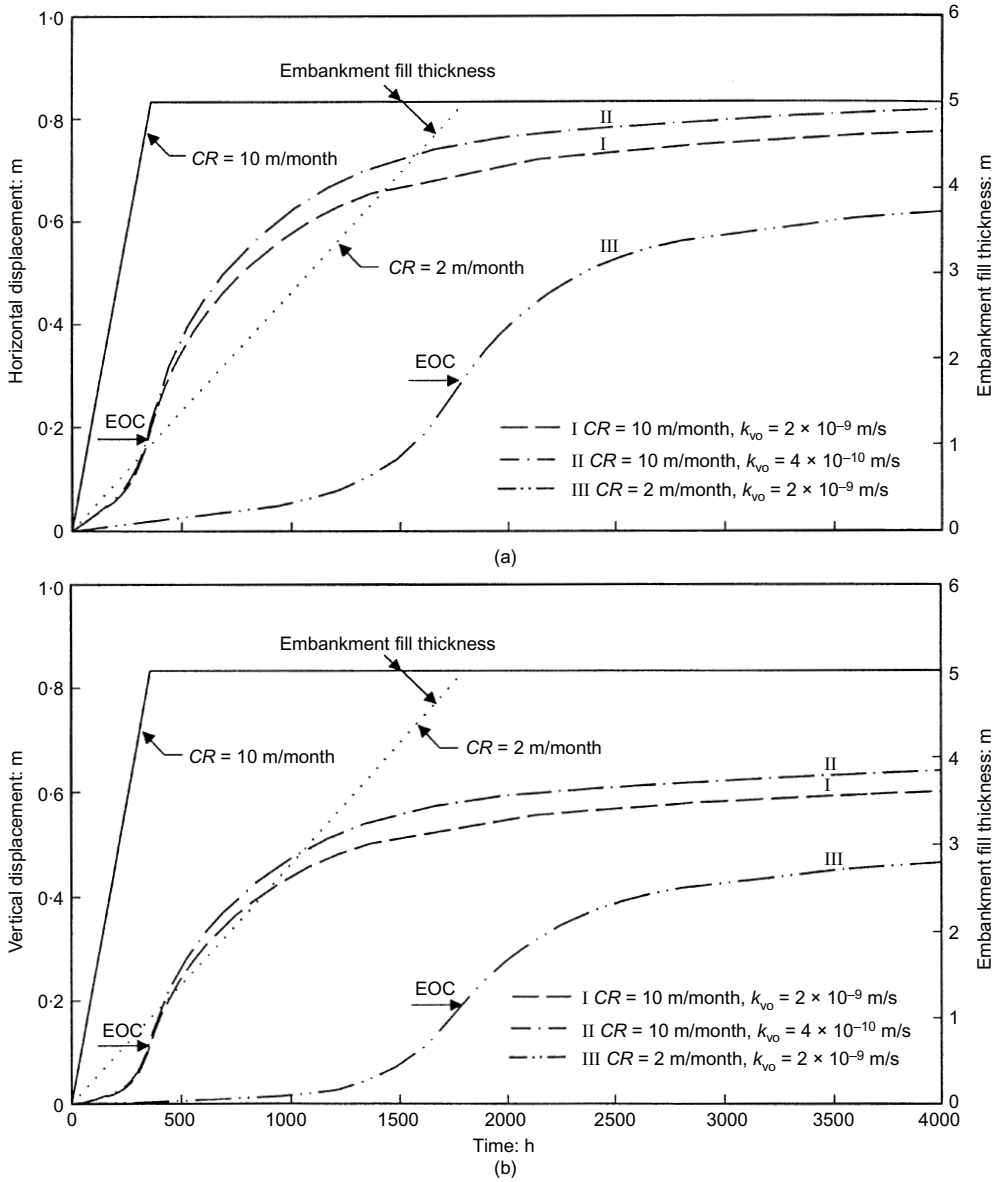

Fig. 9. Deformations at the toe for embankments over soil C-R1 ($H = 5$ m, $J = 2000$ kN/m): (a) horizontal deformations; (b) heave

found to be developed at the location below the embankment centreline owing to the smaller embankment width and wider failure surface than those of the 5 m embankment over soil C-R1.

Effect of reinforcement stiffness

Fig. 12 shows that the development of horizontal deformation at the embankment toe and excess porewater pressure at the location 4·8 m deep and 6·8 m away from the embankment centreline (within the region where maximum pore water pressure develops—see Fig. 11) after the end of construction of 5 m thick unreinforced and reinforced embankments. It was assumed that the reinforcement had sufficient strength to sustain the tensile strain developed without breakage. Fig. 12(a) indicates that the unreinforced embankment had the greatest horizontal toe deformation, and failed about 860 hours after the end of construction. For the reinforced embankments the stiffer the reinforcement the less was the horizontal deformation developed. It is evident that the use of the reinforcement can efficiently confine the creep deformation. It was also found that the reinforcement had no significant effect on the deformations at the end of construction. This implies that for these cases the role of the reinforcement was significant only after construction, during the creep and stress-relaxation period. During this period, the tensile force of reinforcement effectively reduced the creep-induced shearing of viscoplastic foundation soils.

Fig. 12(b) shows that the reinforcement had no significant influence on the excess porewater developed in foundation soil shortly after the end of construction for the cases examined. This is because the soil at this location reached failure shortly after the end of construction in all cases, and in this state the excess pore water was at the same maximum value because the external load was the same (i.e. 5 m fill thickness). However, during the subsequent consolidation the soil moved into a yield state from the failure state owing to the strength gain. Within this state, the use of reinforcement modified the shear intensity in the soil and consequently reduced the creep of the soil. It is noted that the excess pore pressures decrease because of consolidation and increase because of the creep of the foundation soil, and that these two processes can occur simultaneously. Therefore the use of reinforcement influenced the dissipation of the excess pore pressures, as shown in Fig. 12(b). The stiffer the reinforcement the faster the excess pore pressures dissipated; this is due to lower levels of creep-generated pore pressures.

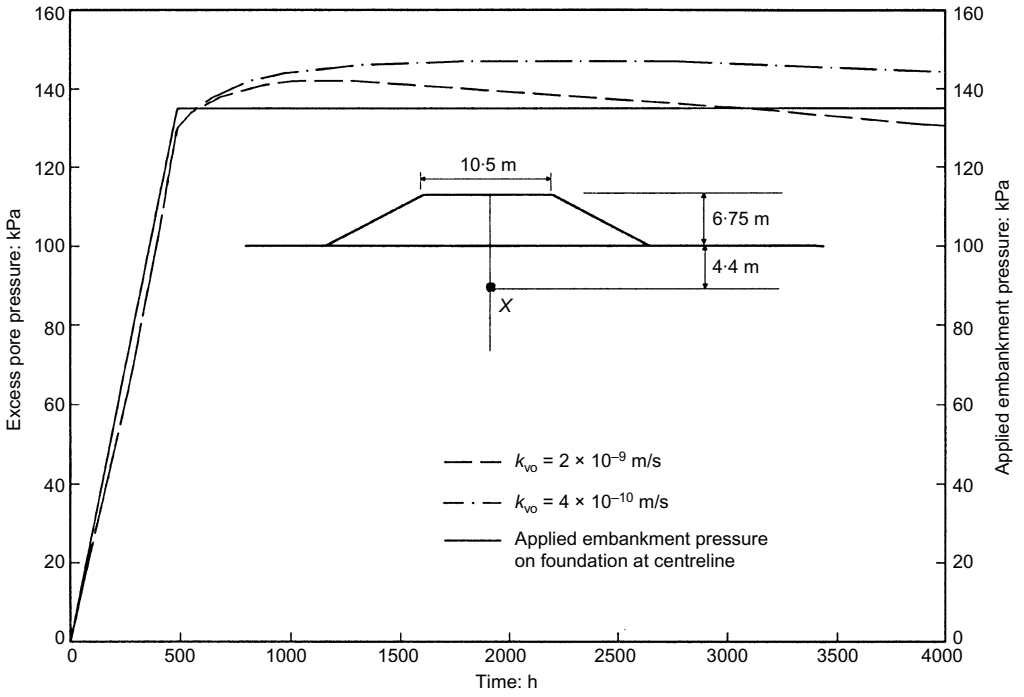

Fig. 10. Maximum excess pore pressure at point X in the foundation soil C-R1 for cases with $H = 6{\cdot}75$ m, $CR = 10$ m/month and $J = 2000$ kN/m

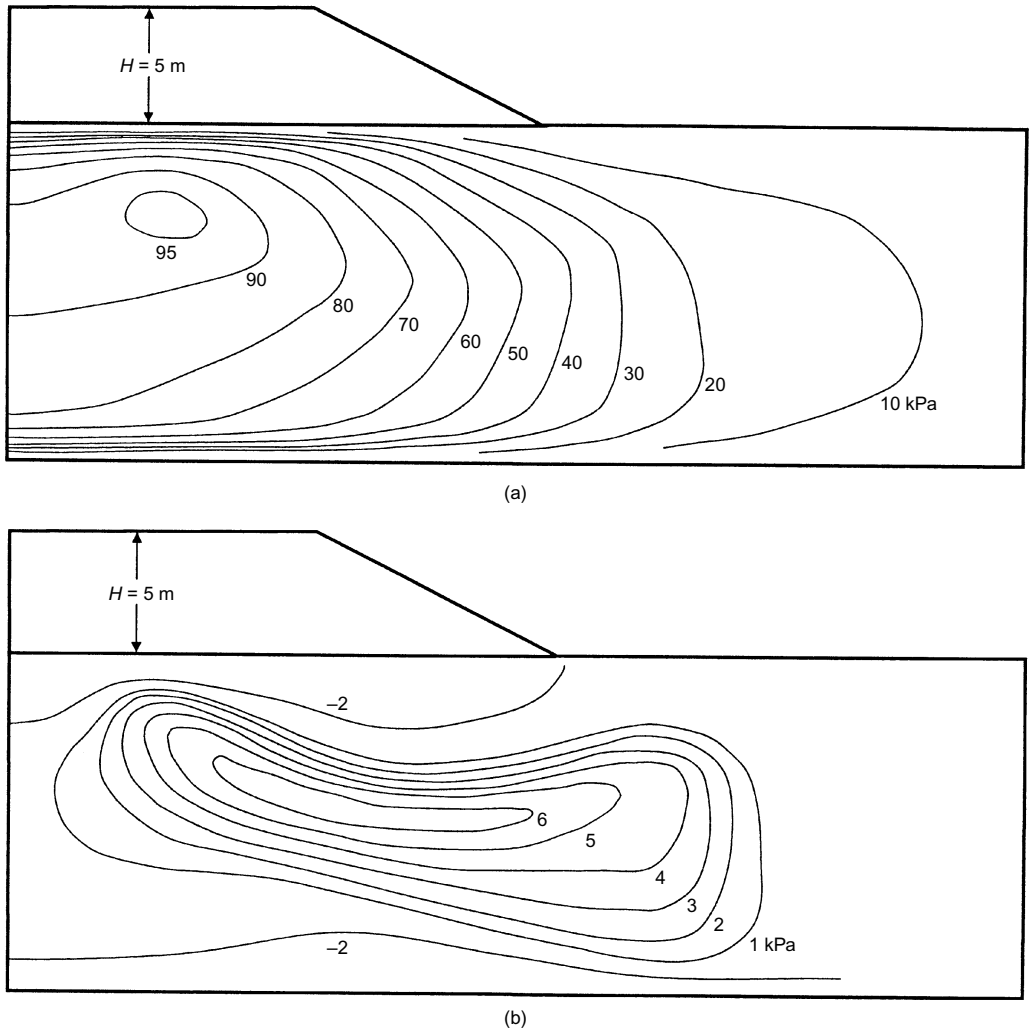

Fig. 11. Contours of excess pore pressures (kPa) for Case I with soil C-R1: (a) total excess pore pressure 455 h (19 days) after EOC; (b) increase in excess pore pressure between EOC and 455 h (19 days) after EOC

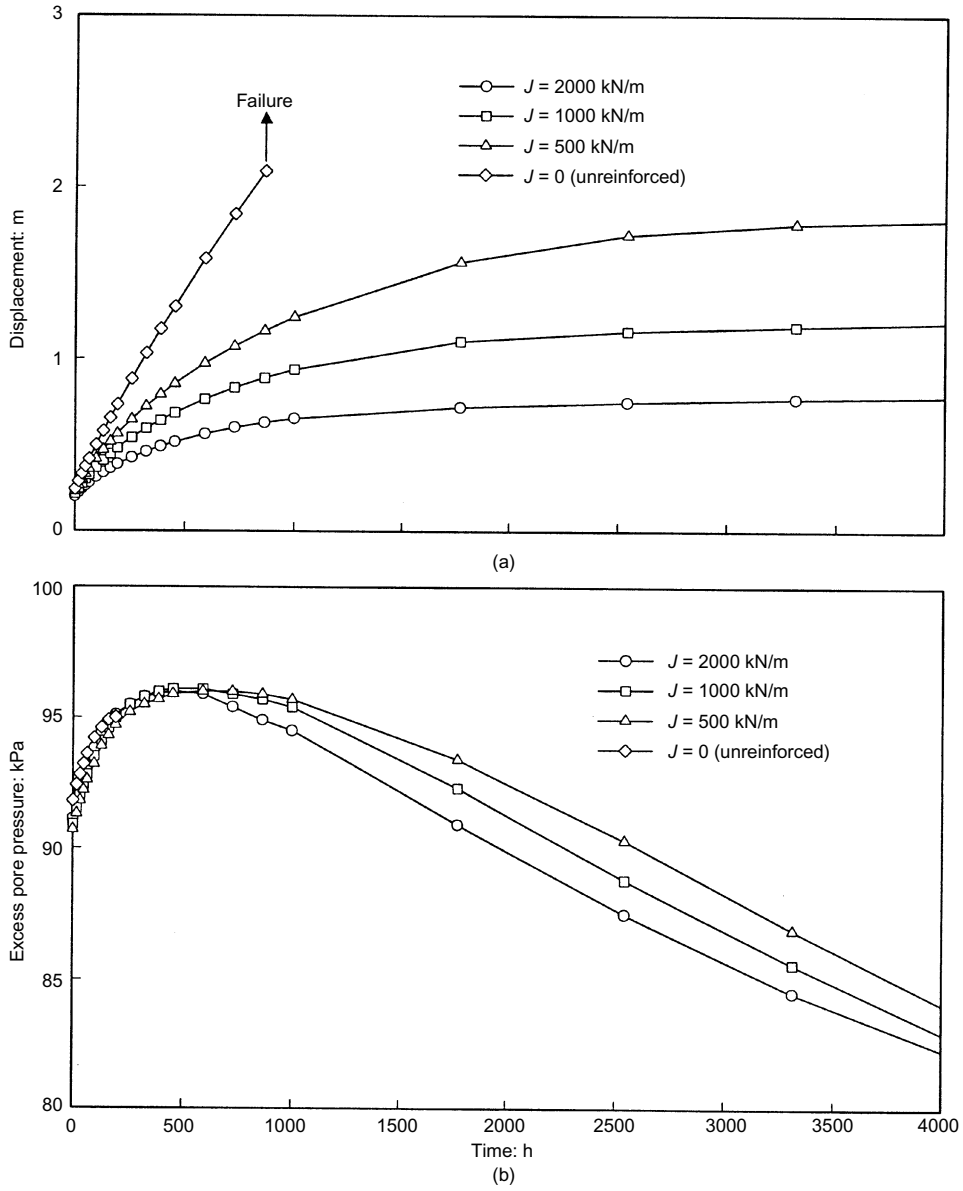

Fig. 12. Effect of reinforcement on pore pressure and creep deformations for cases with $H = 5$ m, $CR = 10$ m/month and soil C-R1 with $k_{vo} = 2 \times 10^{-9}$ m/s: (a) horizontal toe deformation; (b) pore pressure at location 4·8 m deep and 6·8 m away from centreline

SUMMARY AND CONCLUSIONS

The time-dependent behaviour of embankments constructed over rate-sensitive foundation soils has been investigated using a finite element program that can model the soil–reinforcement interaction and viscoplastic characteristics of soil materials. The factors examined include the viscoplastic parameters of soft cohesive soil, reinforcement, construction rate and hydraulic conductivity of soils. When embankments are constructed over rate-sensitive foundation soils at typical construction rates, the viscoplastic behaviour (i.e. creep and stress-relaxation) of foundation soils after the end of construction can have a significant effect on embankment performance, although this can be mitigated by the use of reinforcement. The key findings for the rate-sensitive soils and cases examined can be summarised as follows:

(*a*) The embankment stability after the end of construction is more critical than that at the end of construction. This finding is consistent with observations in a number of field cases where embankments were constructed on rate-sensitive soils (e.g. Keenan *et al.*, 1986; Rowe & Hinchberger, 1998).

(*b*) An arbitrary choice of the strain rate for use in the determination of undrained shear strength may potentially lead to post-construction failure. Special care is needed to select appropriate strength parameters for this type of soil.

(*c*) The maximum reinforcement strain mobilised at the end of construction is relatively small owing to rate effects on the foundation soils during the construction. However, the creep of the foundation soils after the construction can result in a significant increase in reinforcement strain. This finding is also consisted with field observation (Rowe & Hinchberger, 1998). The increase in reinforcement strain after construction was about one to three times the maximum strain mobilised at end of construction based on the finite element results for the cases examined herein.

(*d*) Partial consolidation during and shortly after construction can contribute to a reduction in the maximum reinforcement strain and creep deformations of the foundation soils.

(*e*) The creep of viscoplastic foundation soils under a constant embankment load can result in an increase in excess pore pressure and/or no apparent dissipation in excess pore pressure for significant periods of time after the completion of embankment filling when the drainage conditions do not allow fast dissipation of excess pore pressure. This phenomenon has been observed in a number of field cases (e.g. Crooks *et al.*, 1984; Kabbaj *et al.*, 1988). The time-

dependent response of excess pore pressures is a function of the viscoplastic parameters of foundation soils, the magnitude of the external load, the shearing intensity, embankment geometry, drainage paths, construction rates, and the hydraulic conductivity of the soil.

(*f*) The use of reinforcement can significantly reduce creep deformations of the foundation soils. The stiffer the reinforcement the less the creep deformations that are developed (other things being equal).

ACKNOWLEDGEMENTS

The research reported in this paper was funded by the Natural Sciences and Engineering Research Council of Canada.

NOTATION

C_k	hydraulic conductivity change index
CR	construction rate
$\dot{\varepsilon}_{ij}^{e}$	elastic strain tensor
$\dot{\varepsilon}_{ij}$	strain rate tensor
$\dot{\varepsilon}_{ij}^{vp}$	viscoplastic strain tensor
ε_{all}	allowable reinforcement strain tensor
E	Young's modulus of the soil
ERAT	equilibrium ratio
e	void ratio
e_o	reference void ratio
f	plastic potential function
ψ	dilatancy angle
ϕ'	friction angle
$\Phi(F)$	flow function
G	shear modulus
γ	unit weight
γ^{vp}	fluidity constant of viscous soil
H	embankment thickness
J	reinforcement stiffness
J_2	second invariant of the deviatoric stress tensor
K	bulk modulus
K_0'	coefficient of lateral earth pressure at rest
K_s	material constant of the Janbu's model
k_{v0}	reference hydraulic conductivity
k_v	hydraulic conductivity in the vertical direction
k_h	hydraulic conductivity in the horizontal direction
l	mean effective stress corresponding to the centre of the ellipse
m	material constant of the Janbu's model
$M_{N/C}$	slope of Drucker-Prager failure envelope in normally consolidated stress range
$M_{O/C}$	slope of Drucker-Prager failure envelope in overconsolidated stress range
n	strain rate exponent
OCR	overconsolidated ratio
P_a	atmospheric pressure
κ	recompression index
λ	compression index
υ'	Poisson's ratio
R	aspect ratio
s_u	undrained shear strength
σ_3	minor principal stress
σ_{ij}'	effective stress tensor
σ_p'	preconsolidation pressure
σ_m'	effective mean stress
$\sigma_{os}'^{(d)}$	overstress
σ_v'	vertical effective stress
$\sigma_y'^{(d)}$	dynamic yield surface intercept
$\sigma_y'^{(s)}$	static yield surface intercept
$\sigma_{yA}'^{(s)}$	static yield surface intercept of Point A
$\sigma_{yB}'^{(d)}$	dynamic yield surface intercept of Point B
$\sigma_{yB}'^{(s)}$	static yield surface intercept of Point B
$\sigma_{yC}'^{(s)}$	static yield surface intercept of Point C
t	time

REFERENCES

Biot, M. A. (1941). General theory of three-dimensional consolidation. *J. Appl. Phys.* **12**, 155–164.

Bishop, A. W. & Henkel, D. J. (1962). *The measurement of soil properties in the triaxial test*, 2nd edn. London: Edward Arnold.

Bjerrum, L. (1972). Embankments on soft ground. *Proceedings of the ASCE special conference on earth and earth-supported structures*, Purdue University, West Lafayette, Vol. 2, pp. 1–54.

Carter, J. P. & Balaam, N. P. (1990). *AFENA: A general finite element algorithm: users manual*. School of Civil and Mining Engineering, University of Sydney, Australia.

Casagrande, A. & Wilson, S. D. (1951). Effect of rate of loading on the strength of clays and shales at constant water content. *Géotechnique* **2**, No. 3, 251–263.

Chen, W. F. & Mizuno, E. (1990). *Nonlinear analysis in soil mechanics: theory and implementation*. New York: Elsevier.

Crooks, J. H. A., Becker, D. E., Jeffries, M. G. & McKenzie, K. (1984). Yield behaviour and consolidation. I: Pore pressure response. *Proceedings of the ASCE symposium on sedimentation consolidation models, prediction and validation*, San Francisco, pp. 356–381.

Davis, E. H. (1968). Theories of plasticity and failure of soil masses. In *Soil mechanics: selected topics* (ed. I. K. Lee), Chapter 6. Butterworths.

Fisher, D. G., Rowe, R. K. & Lo, K. Y. (1982). *Prediction of the second stage behaviour of Gloucester test fill. Part 1 – Predictions; Part 2 – Method of analysis*, Geotechnical Research Reports GEOT-3–82, GEOT-4–82. London, Canada: University of Western Ontario.

Fowler, J. & Koerner, R. M. (1987). Stabilisation of very soft soil using geosynthetics. *Proc. Geosynthetic '87 Conf., New Orleans* **1**, 289–299.

Germaine, J. T. & Ladd, C. C. (1988). Triaxial testing of saturated cohesive soils. In *Advanced triaxial testing of soil and rock*, ASTM STP 977, pp. 421–459. Philadelphia: ASTM.

Gibson, R. E. & Lo, K. Y. (1961). *A theory of consolidation of soils exhibiting secondary consolidation*. Oslo. Norwegian Geotechnical Institute No. 41.

Graham, J., Crooks, J. H. A. & Bell, A. L. (1983). Time effects on the stress–strain behaviour of natural soft clays. *Géotechnique* **33**, No. 3, 727–340.

Helwany, M. B. & Wu, J. T. H. (1995). A numerical model for analyzing long-term performance of geosynthetic-reinforced soil structures. *Geosynth. Int.* **2**, No. 2, 429–453.

Hinchberger, S. D. (1996). *The behaviour of reinforced and unreinforced embankments on rate sensitive clayey foundations*. PhD thesis, University of Western Ontario, London, Canada.

Hinchberger, S. D. & Rowe, R. K. (1998). Modelling the rate sensitive characteristics of the Gloucester foundation soil. *Can. Geotech. J.* **35**, No. 5, 769–789.

Holtz, R. D., Christopher, B. R. & Berg, R. R. (1997). *Geosynthetic engineering*. Richmond, British Columbia, Canada: BiTech Publishers.

Industrial Fabrics Association International (1999). 2000 specifier's guide. *Geotechnical Fabrics Report* **10**, No. 7.

Ingold, T. S. (1982). An analytical study of geotextiles reinforced embankments. *Proc. 2nd Int. Conf. Geotextiles*, Las Vegas **3**, 683–688.

Janbu, N. (1963). Soil compressibility as determined by oedometer and triaxial tests. *Proc. Eur. Conf. Soil Mech. Found. Engng*, Wiesbaden **1**, 19–25.

Jewell, R. A. (1996). *Soil reinforcement with geotextiles,* CIRIA Special Publication 123. London: Thomas Telford.

Kabbaj, M., Tavenas, F. & Leroueil, S. (1988). In situ and laboratory stress–strain relationships. *Géotechnique* **38**, No. 1, 83–100.

Keenan, G. H., Landva, A. O., Valsangkar, A. J. & Comier, R. S. (1986). Performance and failure of test embankment on organic silty clay. *Proceedings conference on building on marginal and derelict land*, Glasgow, Vol. 2, pp. 417–428.

Kulhawy, F. H. & Mayne, P. W. (1990). *Manual on estimation soil properties for foundation design*, Electric Power Research Institute Report, California.

Leroueil, S. & Marques, M. E. S. (1996). Importance of strain rate and temperature effects in geotechnical engineering. *Proc. 1996 ASCE Nat. Conv., Washington DC,* Geotechnical Special Publication No. 61, 1–60.

Leshchinsky, D. (1987). Short-term stability of reinforced embankment over clayey foundations. *Soils Found.* **27**, No. 3, 43–57.

Li, A. L. & Rowe, R. K. (1999). Reinforced embankments and the effect of consolidation on soft cohesive soil deposits. *Proc. Geosynthetics '99, Boston* **1**, 477–490.

Lo, K. Y. & Morin, J. P. (1972). Strength anisotropy and time effects of two sensitive clays. *Can. Geotech. J.* **9**, No. 3, 261–277.

Lo, K. Y., Bozozuk, M. & Law, K. T. (1976). Settlement analysis of Gloucester test fill. *Can. Geotech. J.* **13**, No. 4, 339–354.

Mylleville, B. L .J. & Rowe, R. K. (1988). *Simplified undrained stability analysis for use in the design of steel reinforced embankments on soft foundations*, GEOT-3–88. University of Western Ontario, London, Canada.

Perzyna, P. (1963). The constitutive equations for work-hardening and rate sensitive plastic materials. *Proc. Vibrational Problems, Warsaw* **4**, No. 3, 281–290.

Rowe, R. K. & Gnanendran, C. T. (1994). Geotextile strain in a full scale reinforced test embankment. *Geotextiles and Geomembranes* **13**, 781–806.

Rowe, R. K. & Hinchberger, S. D. (1998). The significance of rate effects in modelling the Sackville test embankment. *Can. Geotech. J.* **35**, No. 3, 500–516.

Rowe, R. K. & Li, A. L.(1999). Reinforced embankments over soft foundations under undrained and partially drained conditions. *Geotextiles and Geomembranes* **17**, No. 3, 129–146.

Rowe, R. K. & Soderman, K. L. (1985). An approximate method for estimating the stability of geotextile reinforced embankments. *Can. Geotech. J.* **22**, No 3, 392–398.

Rowe, R. K. & Soderman, K. L. (1987). Stabilisation of very soft soils using high strength geosynthetics: the role of finite element analyses. *Geotextiles and Geomembranes* **6**, No. 1–3, 53–80.

Rowe, R. K., Gnanendran, C. T., Landva, A. O. & Valsangkar, A. J. (1996). Calculated and observed behaviour of a reinforced embankment over soft compressible soil. *Can. Geotech. J.* **33**, No. 2, 324–338.

Sharma, J. S. & Bolton, M. (1996). Centrifuge modelling of an embankment on soft clay reinforced with a geogrid. *Geotextiles and Geomembranes* **14**, No. 1, 1–17.

Sheahan, T. C., Ladd, C. C. & Germaine, J. T. (1996). Rate-dependent undrained shear behaviour of saturated clay. *J. Geotech. Engng* **122**, No. 2, 99–108.